Original research

Glycogen metabolism in an oral dysplastic/cancerous (iodine-negative) epithelium: glycogen was consumed in the pentose phosphate pathway, not in glycolysis

Nobuhiko Yoshimura[a], Shin-ichi Yamada[a,*], Hitoshi Aizawa[a], Tiepeng Xiao[b], Fumihiro Nishimaki[a], Hiroshi Kurita[a]

[a]Department of Dentistry and Oral Surgery, Shinshu University School of Medicine, 3-1-1 Asahi, Matsumoto 390-8621, Japan

[b]Department of Orthodontics, Second Hospital of Hebei Medical University, 050000 Shijiazhuang, China

[*]Corresponding author: Shin-ichi Yamada, DDS, PhD

Department of Dentistry and Oral Surgery

Shinshu University School of Medicine

3-1-1, Asahi, Matsumoto, 390-8621, Japan

Tel.: +81 (0)263-37-2675, Fax: +81 (0)263-37-2676

E-mail: yshinshin@shinshu-u.ac.jp

Running title: Glycogen metabolism in an oral dysplastic/cancerous (iodine-negative) epithelium.

Abstract

The purpose of this study was to investigate differences in glycogen metabolism (glycogen synthesis and glycolysis) between dysplastic/malignant (iodine-negative) and normal (iodine-positive) oral epithelial tissue. Twenty-two frozen samples of iodine-positive and -negative mucosal tissue were obtained from 22 oral squamous cell carcinoma (OSCC) patients. Serial frozen sections were cut and analyzed using hematoxylin-eosin and periodic acid-Schiff methods and immunohistochemical (IHC) staining for glucokinase (GK), phosphoglucomutase 3 (PGM3), and glucose-6-phosphatase (G6Pase) to investigate glycogen metabolism. The expression levels of metabolites in OSCC and normal oral epithelial tissue were subjected to a metabolome analysis to clarify differences in central carbon metabolism, including glycogen metabolism. No significant differences were observed in GK or PGM3 immunoactivity between iodine-positive and -negative areas. However, G6Pase immunoreactivity was significantly stronger in the upper layers of the negative epithelium. In the metabolome analysis, significant differences were noted in the last half of glycolysis. Lactic acid as the final metabolite in glycolysis was detected in the dysplastic/cancerous oral epithelium, and its levels were slightly higher than those in the normal epithelium. G6Pase expression was significantly strong in dysplastic/cancerous oral epithelial cells. Dysplastic/cancerous oral epithelial cells exhibited stronger activation for glucose metabolism. The results of the metabolome analysis suggest that glucose and glycogen degradation products in oral dysplastic/cancerous epithelial cells are used for nucleic acid synthesis through the pentose phosphate pathway.

Keywords:

Oral squamous cell carcinoma, Glycogen metabolism, Iodine vital staining, Glucose-6-phosphatase, metabolome analysis

1. Introduction

Oral squamous cell carcinoma (OSCC) is the most frequent malignant neoplasm of the oral cavity [1]. An adequate surgical margin for primary tumor resection is one of the important prognostic factors for recurrence and overall survival in OSCC treatment strategies [2-5]. However, regarding surgical margins, difficulties are associated with distinguishing between the normal epithelium and dysplastic/cancerous epithelium using conventional visual examinations and palpation.

Vital staining with iodine solution has been widely used to distinguish the dysplastic/cancerous oral epithelium from normal mucosa and its usefulness has been demonstrated [6-9]. Iodine reacts with glycogen in the cytoplasm of the oral epithelium [4]. Iodine solution reacts with the normal non-keratinized squamous epithelium, but not severely dysplastic or malignant epithelial tissue due to differences in the glycogen content of the cytoplasm between these tissues [4,10-12]. An oral epithelium exhibiting dysplastic changes with a high potential for malignant transformation has been reported to contain reduced amounts of glycogen [4,6,7]. Additionally, glucose consumption is known to be markedly increased in oral dysplastic/cancerous epithelial cells. Glycogen is regarded as “a store of glucose” and may also be depleted. However, glycogen metabolism, such as glycogen synthesis and glycogenolysis, has not yet been examined in detail in oral dysplastic/cancerous epithelial cells [4,12,13].

We previously reported elevated glucose uptake (the activation of glucose transporter 1 (GLUT-1) and enhanced glycogenolysis (activation of glycogen phosphorylase) in iodine-negative areas, such as dysplastic/cancerous oral epithelial

cells [4,13]. However, it currently remains unclear whether glucose 6-phosphate (G6P), which is derived from the disassembly of intracellular glucose or glycogen, proceeds to glycolysis or the pentose phosphate pathway (Fig. 1). Therefore, the purpose of this study was to investigate glucose-1 phosphate (G1P) and G6P metabolism (*i.e.* phosphoglucomutase, glucokinase (GK), and glucose 6-phosphatase (G6Pase)) as well as the activities of glycolysis and the pentose phosphate pathway in oral dysplastic/cancerous (iodine-negative) epithelial tissue using a metabolome analysis.

2. Materials and methods

2.1. Patients

Between June 2011 and September 2014, 55 consecutive patients with histologically proven primary OSCC were examined. Twenty-two samples from these patients, including iodine-positive and -negative areas, successfully subjected to a frozen section analysis were included in this study. Written informed consent was obtained from all patients before their inclusion, and the study was approved by the Ethics Committee of the Shinshu University School of Medicine (No.1341).

2.2. Histology and immunohistochemistry

Dental iodine glycerin (10 mg iodine/100 ml; Showa Yakuhin, Japan) was used as the vital staining solution before primary tumor resection. Tissue around lesions was stained with iodine as described below: 1; confirm whether a patient has an iodine allergy, 2; rinse with water and dry the surface of the mucosa, 3; apply dental iodine glycerin with a cotton bud and dye the lesion of the mucosa, and 4; wait for 1 to 2 minutes and then assess the staining reaction. After iodine vital staining, specimens that included iodine-positive and -negative areas were obtained from the boundary region.

All specimens were stored at -80°C after being snap-frozen in dry ice-cooled acetone[4]. Five-μm-thick frozen serial sections were cut and mounted on Matsunami adhesive silane-coated glass slides (Matsunami Glass, Japan). The first vital section was placed in xylene for 30 s after being subjected to 30 min of air drying at room temperature, and was then mounted onto a coverslip. These slides were subjected to light microscopic examinations and microphotography as soon as possible because the brown-black color of iodine gradually disappears over the course of 2 weeks. Other sequential sections were subjected to hematoxylin and eosin (H&E) and periodic acid-Schiff (PAS) staining. To ensure optimal cell structure preservation and that tissue sections remained sensitive to immunostaining, 20% formalin neutral buffer solution was used to fix sections, which were then subjected to a 12-min microwave treatment in Tris/ethylenediamine tetraacetic acid (pH 8.0) for antigen retrieval. Normal serum blocking and the exclusion of the primary antibody were used to produce negative controls. Immunoreactivity was visualized with diaminobenzidine and hydrogen peroxide [4,13]. The antibodies used in the present study included anti-GK (an enzyme that facilitates the phosphorylation of glucose to glucose-6-phosphate, a glycogen synthesis marker; 1:100 dilution; GCK, Thermo Fisher Scientific, Waltham, MA, USA), phosphoglucomutase 3 (PGM3) (an enzyme that catalyzes the interconversion of G1P and G6P, glycogen synthesis and glycolysis markers; 1:100 dilution; EC13, Santa Cruz Biotechnology, Dallas, TX, USA), and G6Pase (an enzyme that hydrolyzes glucose-6-phosphate, resulting in the creation of free glucose, a glycolysis marker; 1:100 dilution; ab76598, Abcam, UK) antibodies.

In the histochemical assessment, the oral epithelium was divided into three compartments: the basal, parabasal, and superficial layers, as described previously[14].To investigate differences in the expression levels of molecules (*i.e.* GK,

PGM3, and G6Pase) between iodine-positive and -negative epithelial tissues, the percentages of cells that were positive for GK (membranous), PGM3 (membranous), and G6Pase (membranous) in each layer were calculated in a 400× field (five fields per area), irrespective of the intensity of staining. In each area, the first field was placed close to the boundary between iodine-positive and -negative areas, and the other four fields were randomly selected. Since the use of iodine vital staining was reported to be limited to the mucosal and normally non-keratinized mucosa [8], especially in gingiva cases, non-keratinized lesions were assessed. All slides were reviewed and assessed by two independent observers, and the mean positive cell count was calculated [4,13].

2.3. Sample collection and metabolite extraction

Oral dysplastic/cancerous and the surrounding grossly normal epithelial tissues were obtained from 10 randomly selected (out of 22) patients in the present study after surgery. Excised tissues were cut into < 1-cm^3 pieces, immediately frozen in liquid nitrogen, and stored at - 80 ºC until metabolite extraction. Each frozen sample was homogenized in methanol, and metabolites were extracted for an analysis by CE-MS. Metabolite extraction and the metabolome analysis were conducted at Human Metabolome Technologies (HMT; Tsuruoka, Yamagata, Japan). Briefly, approximately 50 mg of frozen tissue was placed into 1,500 μL of 50% acetonitrile/Milli-Q water containing internal standards (Solution ID: 304-1002, HMT) at 0 ºC in order to inactivate enzymes. The tissue was homogenized six times at 4,000 rpm for 60 s using a tissue homogenizer (Micro Smash MS100R, Tomy Digital Biology Co., Ltd., Tokyo, Japan), and the homogenate was then centrifuged at 2,300×*g* at 4ºC for 5 minutes. Eight hundred microliters of the upper aqueous layer was centrifugally filtered through a Millipore 5-kDa cut-off filter at 9,100 ×*g* at 4 ºC for 120 minutes to remove proteins.

The filtrate was centrifugally concentrated and re-suspended in 50 μL of Milli-Q water for the CE-MS analysis at HMT.

2.4. Metabolome analysis

The metabolome analysis was conducted using the *Basic Scan* package of HMT with capillary electrophoresis time-of-flight mass spectrometry (CE-TOFMS) based on previously described methods [15,16]. Briefly, a CE-TOFMS analysis was performed using an Agilent CE capillary electrophoresis system equipped with an Agilent 6210 time-of-flight mass spectrometer, Agilent 1100 isocratic HPLC pump, Agilent G1603A CE-MS adapter kit, and Agilent G1607A CE-ESI-MS sprayer kit (Agilent Technologies, Waldbronn, Germany). The systems were controlled by Agilent G2201AA ChemStation software version B.03.01 for CE (Agilent Technologies) and connected by a fused silica capillary (50 μm *i.d.* × 80 cm total length) with commercial electrophoresis buffer (H3301-1001 and H3302-1021 for the cation and anion analyses, respectively, HMT) as the electrolyte. The spectrometer was scanned from *m/z* 50 to 1,000. Peaks were extracted using MasterHands automatic integration software (Keio University, Tsuruoka, Yamagata, Japan) to obtain peak information including *m/z*, the peak area, and migration time (MT) [17]. Signal peaks corresponding to isotopomers, adduct ions, and other product ions of known metabolites were excluded, and the remaining peaks were annotated according to the HMT metabolite database based on their *m*/*z* values with MT. The areas of the annotated peaks were then normalized based on internal standard levels and sample amounts. The absolute concentrations of each metabolite were obtained by a one-point calibration using each standard metabolite. A hierarchical cluster analysis (HCA) and principal component analysis (PCA) were

performed by HMT's proprietary software, PeakStat and SampleStat, respectively. Detected metabolites were plotted on metabolic pathway maps using VANTED software [18].

2.5 .Statistical analysis

Data were analyzed with GraphPad Prism (GraphPad Software, Inc., La Jolla, CA, USA) for Windows. Differences in the percentage of positive cells between iodine-positive and -negative areas in each layer of the epithelium were assessed using the Wilcoxon signed-rank test. Welch's *t*-test was used for CE-TOFMS measurements. $P<0.05$ was considered to indicate a significant difference.

3. Results

3.1. Iodine penetration and PAS reactions

Twenty-two patients (12 males and 10 females) were included in this study. The median age of patients was 73 years (range: 26-92 years). The most frequent site of the primary tumor was the tongue in 13 patients (59.1%), gingiva 8 (36.4%), and floor of the mouth 1 (4.5%). In all patients, a histopathological diagnosis of squamous cell carcinoma was established by a pathologist. In iodine vital staining, the iodine-positive areas of the epithelium were characterized by a brown-black color, whereas negative areas were normal in color. In the examination of frozen sections, iodine solution had gradually penetrated the tissue from the surface. The brown-black color did not reach the basal layer in any case (Fig. 2A). However, in the negative area, iodine solution scattered in dysplastic/cancerous epithelial cells.

Iodine-positive and -negative epithelial tissue regions were compared in H&E-

and PAS-positive slides. In H&E-positive sections, a clear difference was observed between the atypical epithelium and normal epithelium (Fig. 2B). Iodine-positive tissue was defined as normal non-keratinized epithelial tissue, while iodine-negative tissue included OSCC and dysplastic tissue according to the WHO classification criteria (2005). In PAS-positive sections, large numbers of glycogen granules were noted in the superficial layers of iodine-positive areas (Fig. 2C). Glycogen granules were distributed throughout the superficial layers, whereas iodine was mainly observed in the upper third of the superficial layer. PAS staining indicated that the distribution of glycogen was similar to that of iodine in the upper superficial layer. However, in the iodine-negative area, there was only a scattering of glycogen granules in the dysplastic/cancerous epithelium that mostly corresponded to the presence of iodine solution.

3.2. Immunohistochemical study

The expression of GK, PGM3, and G6Pase in histochemical staining was shown in Figures 3-5 (Fig. 3-5). GK, PGMS, and G6Pase staining was mainly detected in the basal and parabasal layers in the iodine-positive normal epithelium, and these molecules exhibited similar staining patterns in each layer of iodine-negative dysplastic/cancerous epithelial tissue.

A statistical comparison between the GK positivity rates of cells in iodine-positive and -negative areas is shown in Figure 3C (iodine-positive vs. iodine-negative areas: basal layer, 48.2 vs. 51.9%; parabasal layer, 46.2 vs. 46.5%; superficial layer, 29.8 vs. 34.8%; not significant (NS)). A statistical comparison between the PGM3-positive rates of cells in iodine-positive and -negative areas is shown in Figure 4C (iodine-positive vs. iodine-negative areas: basal layer, 28.5 vs. 23.5%;

parabasal layer, 28.3 vs. 23.7%; superficial layer, 14.6 vs. 20.9%; NS). A statistical comparison between the G6Pase-positive rates of cells in iodine-positive and -negative areas is shown in Figure 5C (iodine-positive vs. iodine-negative areas: basal layer, 50.9 vs. 70.7%; parabasal layer, 46.7 vs. 66.0%; superficial layer, 22.4 vs. 55.1%; $P<0.01$). Significant differences in G6Pase expression were detected in all layers. G6Pase-positive rates were higher in iodine-negative areas than in iodine-positive areas.

3.3. CE-TOFMS measurement

A metabolome analysis was performed to examine differences in metabolites between normal epithelial cells (iodine-positive area) and OSCC cells (iodine-negative area) (Fig. 6). In central carbon metabolism, significant differences were observed in the last half of glycolysis, including glyceraldehyde-3-phosphate (GAP), 3-phosphoglyceric acid (3PG), 2-phosphoglyceric acid (2PG), and phosphoenolpyruvic acid (PEP), which were not detected in the dysplastic/cancerous oral epithelium (iodine-negative area). However, lactic acid, which is the final metabolite in glycolysis, was detected in the dysplastic/cancerous oral epithelium (iodine-negative area), and its levels were slightly higher than those in the normal epithelium (23,510 +- 7,380 vs 18,070 +- 11,304 nmol/g, NS).

In the pentose phosphate pathway, no significant differences were observed between metabolites; however, the concentrations of 6-phosphogluconic acid (6PG), sedoheptulose 7-phosphate (S7P), and phosphoribosyl 1-diphosphate (PRPP) were higher in the dysplastic/cancerous oral epithelium (iodine-negative area) than in the normal epithelium (6PG, 28 +- 36 vs 20 +- 12 nmol/g, NS; S7P, 28 +- 12 vs 20 +- 11 nmol/g, NS; and PRPP, 7.3 +- 7.9 vs 6.3 +- 3.1 nmol/g, NS). This pathway supplies products that are used in the synthesis of nucleotides and nucleic acids. In the

assessment of purine metabolism, a significantly higher concentration of guanine was observed in the dysplastic/cancerous epithelium than in the normal epithelium (57 +- 27 vs 23 +- 18 nmol/g, $p < 0.01$).

In the TCA cycle, the concentrations of metabolites (succinic acid, fumaric acid, and citric acid) were slightly higher in the dysplastic/cancerous epithelium than in the normal epithelium. Slightly or significantly higher concentrations of glutamic acid, arginine, aspartic acid, and alanine, which are involved in the glutaminolytic pathway, were observed in the dysplastic/cancerous epithelium than in the normal epithelium (glutamic acid, 3,969 +- 981 vs 1,430 +- 799 nmol/g, $p < 0.01$; arginine, 295 +- 118 vs 181 +- 67 nmol/g, $p <0.05$; aspartic acid, 1,152 +- 480 vs 320 +- 255 nmol/g, $p < 0.01$; alanine, 1,899 +- 557 vs 1,429 vs 495 nmol/g, $p=0.06$). Lactic acid is also the final metabolite in the glutaminolytic pathway, and pyruvate and lactate may be converted from malate.

4. Discussion

G6Pase is one of the key enzymes in glucose homeostasis and catalyzes the hydrolysis of G6P to glucose and phosphate via gluconeogenesis and glycogenolysis [19]. In normal tissues, significant G6Pase activity has been reported to correlate with the rapid clearance of titrated deoxyglucose [20]. Previous studies reported that the expression level of G6Pase was lower in cancer cells than in liver or kidney cells [21,22]. In contrast to these findings, significant differences in G6Pase expression were detected in all layers between iodine-positive and -negative areas in the present study. These results suggest that the dysplastic/cancerous oral epithelium exhibited stronger activation for the utilization of glucose through the enzyme activation of G6Pase. Glycogen consumption may have been increased in the upper layer of the

dysplastic/cancerous oral epithelium.

Phosphoglucomutases (PGM) are members of the hexose-phosphate mutase family and involved in the interconversion of glucose-1-phosphate to glucose-6-phosphate [23]. PGM activity is essential for the formation of glycogen and the carbohydrate chains of glycoproteins through the conversion of G6P to G1P [23]. The reverse reaction of G1P to G6P is the main pathway for glycogen utilization followed by glycolysis and gluconeogenesis [23]. PGM3 is one of the five isoenzymes of PGMs [23]. In prostate cancer, PGM3 has been reported to play a role in the regulation of cancer cell survival [24]. In the present study, the number of PGM3-positive cells was slightly higher in iodine-negative areas than in iodine-positive areas in the superficial and parabasal layers. In our previous study [13], significant GPBB expression was detected in both the basal and parabasal layers, and a similar pattern was observed for p53 and Ki67 staining in the iodine-negative oral epithelium. Glycogenolysis was activated in the basal and parabasal layers in the dysplastic/cancerous oral epithelium because of the increased proliferation of malignant potential cells. In addition, increased glycogen consumption accompanied by enhanced G6Pase expression in the upper layer of dysplastic/cancerous oral epithelium may be involved in the development of the iodine-negative region in the dysplastic/cancerous oral mucosal epithelium.

In the 1920s, Otto Warburg observed the accumulation of lactate during glucose metabolism in ascites cancer cells, even in the presence of abundant amounts of oxygen [25]. Increased glucose uptake, a shift in pyruvate oxidative phosphorylation in the mitochondria towards a more rapid aerobic glycolysis even in a normoxic environment, and the increased conversion of pyruvate to lactate are collectively known as the Warburg effect or aerobic glycolysis, and is a common metabolic characteristic of

cancer cells [26]. However, in the present study, the results of the metabolome analysis showed that GAP, 3PG, 2PG, and PEP, which were metabolites in the last half of glycolysis, were not detected in the dysplastic/cancerous oral epithelium, whereas pyruvic acid and lactate were present. Glucose metabolism yields ribose for nucleic acid synthesis and NADPH through the pentose phosphate pathway, while glycolysis provides intermediates to maintain anaplerosis and supply biosynthetic intermediates [27]. Glucose uptake and glycogenolysis are advantageous for proliferating cancer cells by favoring the utilization of the most abundant energy and carbon sources. The present results showed that 6PG, S7P, R5P, and PRPP, which are intermediates in the pentose phosphate pathway, were present in the dysplastic/cancerous oral epithelium. Furthermore, a significantly higher concentration of guanine was observed in purine metabolism. These results suggest that G6P, a key intermediate in glucose and glycogen metabolism, is mainly used in the pentose phosphate pathway, not in glycolysis in oral cancerous tissue.

A previous study reported that cancer cells use not only glucose, but also glutamine as an additional energy source [28]. The metabolic pathway from glutamine to lactate is known as glutaminolysis [29]. In the present study, a significantly higher concentration of glutamine was noted in the oral dysplastic/cancerous epithelium. The concentrations of metabolites, including succinic acid, fumaric acid, and citric acid, were slightly higher in the dysplastic/cancerous epithelium than in the normal epithelium. Furthermore, slightly or significantly higher concentrations of glutamic acid, arginine, aspartic acid, and alanine, which are involved in the glutaminolytic pathway, were observed in the dysplastic/cancerous epithelium than in the normal epithelium. These results suggest that glutaminolysis occurs in oral dysplastic/cancerous tissue. The accumulation of lactate and pyruvic acid in the dysplastic/cancerous epithelium may

have been due to enhanced glutaminolysis rather than glycolysis. Glutamine and its degradation products glutamate and aspartate are precursors for nucleic acid and serine synthesis. Glutamine is critical for many fundamental cell functions in cancer cells, including the synthesis of metabolites that maintain mitochondrial metabolism, the generation of antioxidants to remove reactive oxygen species, the synthesis of non-essential amino acids, purines, pyrimidines, and fatty acids for cellular replication, and the activation of cell signaling [30]. The activation of glutaminolysis may be advantageous for proliferating cancer cells.

Based on the present results, G6P, a key intermediate in glucose and glycogen metabolism, appears to be used in the pentose phosphate pathway, but not in glycolysis in oral cancerous tissue because there were no intermediate metabolites of the last half of glycolysis. Glycogen was consumed in the pentose phosphate pathway, but not in glycolysis. G6P was also used for gluconeogenesis, possibly to store energy and carbon sources in oral dysplastic/cancerous tissue. Since glutaminolysis is activated in the oral dysplastic/cancerous epithelium, our results suggest that the accumulation of lactic acid is due to enhanced glutaminolysis, not glycolysis.

The present study is the first to investigate differences in glycogen metabolism between iodine-negative dysplastic/cancerous oral epithelial tissue and iodine-positive normal oral epithelial tissue based on immunohistochemical and metabolome analyses. The limitation of this study was that the results obtained were based on a relatively small number of cases at a single institute. Large variations were reported in the metabolome analysis, possibly due to the small sample size, site-specific differences in tissue structures, and the co-existence of cancerous and normal tissues [9]. Therefore, further studies on a large number of cases are needed.

5. Conclusion

Significantly stronger G6Pase expression in all layers was detected in dysplastic/cancerous oral epithelial cells than in normal oral epithelial cells. The dysplastic/cancerous oral epithelium exhibited stronger activation for glucose metabolism. The results of the metabolome analysis suggest that glucose and glycogen degradation products in the oral dysplastic/cancerous epithelium are used for nucleic acid synthesis through the pentose phosphate pathway.

Declarations

Funding: None.

Competing Interests: None.

Ethical Approval: This study was approved by the Committee on Medical Research of Shinshu University (No.1341).

Patient Consent: not required.

References

[1] Jemal A, Bray F, Center MM, Ferlay J, Ward E, Forman D. Global cancer statistics. CA Cancer J Clin 2011;61(2):69-90.

[2] Binahmed A, Nason RW, Abdoh AA. The clinical significance of the positive surgical margin in oral cancer. Oral Oncol. 2007; 43(8):780-4.

[3] Kurita H, Nakanishi Y, Nishizawa R, Xiao T, Kamata T, Koike T, et al. Impact of different surgical margin conditions on local recurrence of oral squamous cell carcinoma. Oral Oncol 2010;46(11):814-7.

[4] Xiao T, Kurita H, Shimane T, Nakanishi Y, Koike T. Vital staining with iodine solution in oral cancer: iodine infiltration, cell proliferation, and glucose transporter 1. Int J Clin Oncol 201318(5):792-800.

[5] Yamada S, Kurita H, Shimane T, Kamata T, Uehara S, Tanaka H, et al. Estimation of the width of free margin with a significant impact on local recurrence in surgical resection of oral squamous cell carcinoma. Int J Oral Maxillofac Surg 2016;45(2):147-52.

[6] Chisholm EM, Williams SR, Leung JW, Chung SC, Van Hasselt CA, Li AK. Lugol's iodine dye-enhanced endoscopy in patients with cancer of the oesophagus and head and neck. Eur J Surg Oncol 1992;18(6):550-2.

[7] Epstein JB, Scully C, Spinelli J. Toluidine blue and Lugol's iodine application in the assessment of oral malignant disease and lesions at risk of malignancy. J Oral Pathol Med 1992;21(4):160-3.

[8] Kurita H, Kurashina K. Vital staining with iodine solution in delineating the border of oral dysplastic lesions. Oral Surg Oral Med Oral Pathol Oral Radiol Endod 1996;81(3):275-80.

[9] Ohta K, Ogawa I, Ono S, Taki M, Mizuta K, Miyauchi M, et al.Histopathological

evaluation including cytokeratin 13 and Ki-67 in the border between Lugol-stained and -unstained areas. Oncol Rep 2010; 24(1):9-14.

[10] Dawsey SM, Fleischer DE, Wang GQ, Zhou B, Kidwell JA, Lu N, et al. Mucosal iodine staining improves endoscopic visualization of squamous dysplasia and squamous cell carcinoma of the esophagus in Linxian, China. Cancer 1998;83(2):220-31.

[11] Nakanishi Y, Ochiai A, Shimoda T, Yamaguchi H, Tachimori Y, Kato H, et al. Epidermization in the esophageal mucosa: unusual epithelial changes clearly detected by Lugol's staining. Am J Surg Pathol 1997;21(5):605-9.

[12] Ogawa T, Washio J, Takahashi T, Echigo S, Takahashi N. Glucose and glutamine metabolism in oral squamous cell carcinoma: insight from a quantitative metabolomic approach. Oral Surg Oral Med Oral Pathol Oral Radiol 2014;118(2):218-25.

[13] Aizawa H, Yamada S, Xiao T, Shimane T, Hayashi K, Qi F, et al. Difference in glycogen metabolism (glycogen synthesis and glycolysis) between normal and dysplastic/cancerous oral epithelium. Arch Oral Biol 2017;83:340-7.

[14] Liu SC, Sauter ER, Clapper ML, Feldman RS, Levin L, Chen SY, et al. Markers of cell proliferation in normal epithelia and dysplastic leukoplakias of the oral cavity. Cancer Epidemiol Biomarkers Prev 1998;7(7):597-603.

[15] Ohashi Y, Hirayama A, Ishikawa T, Nakamura S, Shimizu K, Ueno Y, et al. Depiction of metabolome changes in histidine-starved Escherichia coli by CE-TOFMS. Mol Biosyst 2008;4(2):135-47.

[16] Ooga T, Sato H, Nagashima A, Sasaki K, Tomita M, Soga T, et al. Metabolomic anatomy of an animal model revealing homeostatic imbalances in dyslipidaemia. Mol Biosyst 2011;7(4):1217-23.

[17] Sugimoto M, Wong DT, Hirayama A, Soga T, Tomita M. Capillary electrophoresis mass spectrometry-based saliva metabolomics identified oral, breast and pancreatic cancer-specific profiles. Metabolomics 2010;6(1):78-95.

[18] Junker BH, Klukas C, Schreiber F. VANTED: a system for advanced data analysis and visualization in the context of biological networks. BMC Bioinformatics. 2006 Mar 6;7:109.

[19] Chou JY, Mansfield BC. Mutations in the glucose-6-phosphatase-alpha (G6PC) gene that cause type Ia glycogen storage disease. Hum Mutat 2008;29(7):921-30.

[20] Oshida M, Uno K, Suzuki M, Nagashima T, Hashimoto H, Yagata H, et al. Predicting the prognoses of breast carcinoma patients with positron emission tomography using 2-deoxy-2-fluoro[18F]-D-glucose. Cancer 1998;82(11):2227-34.

[21] Kuang Y, Schomisch SJ, Chandramouli V, Lee Z. Hexokinase and glucose-6-phosphatase activity in woodchuck model of hepatitis virus-induced hepatocellular carcinoma. Comp Biochem Physiol C Toxicol Pharmacol 2006;143(2):225-31.

[22] Smith TA, Sharma RI, Thompson AM, Paulin FE. Tumor 18F-FDG incorporation is enhanced by attenuation of P53 function in breast cancer cells in vitro. J Nucl Med 2006;47(9):1525-30.

[23] Pang H, Li Z, Wang B, Ding M. Polymorphic analysis of the human phosphoglucomutase-3 gene based on mismatched PCR-RFLP technique. Biochem Genet 2010;48(3-4):208-14.

[24] Lee CH, Jeong SJ, Yun SM, Kim JH, Lee HJ, Ahn KS, et al. Down-regulation of phosphoglucomutase 3 mediates sulforaphane-induced cell death in LNCaP prostate cancer cells. Proteome Sci 2010;8:67.

[25] Warburg O, Posener K, Negelein E. Ueber den stoffwechsel der Tumoren [in

German]. Z Biochem 1924;152:319-44.

[26] Warburg O. On the origin of cancer cells. Science 1956;123:309-14.

[27] Vander Heiden MG, Cantley LC, Thompson CB. Understanding the Warburg effect: The metabolic requirements of cell proliferation. Science 2009;324:1029–33.

[28] Coles NW, Johnstone RM. Glutamine metabolism in Ehrlich ascites-carcinoma cells. Biochem J 1962;83:284-91.

[29] Gao P, Tchernyshyov I, Chang TC, Lee YS, Kita K, Ochi T, et al. c-Myc suppression of miR-23a/b enhances mitochondrial glutaminase expression and glutamine metabolism. Nature 2009;458:762-5.

[30] Yang L, Venneti S, Nagrath D. Glutaminolysis: A Hallmark of Cancer Metabolism. Annu Rev Biomed Eng 2017;19:163-94.

Figure legends

Fig. 1 Central carbon metabolism

Glycogenesis produces glycogen from glucose. Glycogenolysis involves the breakdown of glycogen back to glucose. Glycogenesis and glycogenolysis occur in the cell cytoplasm.

Fig. 2 Serial histopathological sections of a surgical margin specimen including iodine-positive (normal) and -negative (severe dysplastic) areas

The arrowhead indicates the boundary between iodine-positive and -negative areas.

(a) No staining: a clear boundary was observed between the iodine-negative (left) and -positive areas (right).

(b) Hematoxylin and eosin (H&E) staining: two distinct histopathological expression patterns that closely mirrored those produced by iodine staining were noted.

(c) Periodic acid–Schiff (PAS) staining: large numbers of glycogen granules were observed in the iodine-positive epithelium, but not in the iodine-negative epithelium.

(a)–(c) Magnification: ×16

Fig. 3 Immunoreactivity of glucokinase (GK).

(A) and (B): Immunohistochemical expression of GK. (C): Comparison of the cell positivity rates of GK for each epithelial layer between the iodine-positive and -negative areas.

(A) Magnification: ×40, (B) Magnification: ×100

The arrowhead indicates the boundary between the iodine-positive and -negative areas.

No significant differences were observed in GK-positive cell rates in each layer between the iodine-positive and -negative areas (Wilcoxon signed-rank test).

Iodine (+), iodine-positive area; iodine (-), iodine-negative area

Fig. 4 Immunoreactivity of glucose-6-phosphatase (G6P).

(A) and (B): Immunohistochemical expression for G6P. (C): Comparison of the cell positivity rates for G6P in each epithelial layer between iodine-positive and -negative areas.

(A) Magnification: ×40, (B) Magnification: ×100

The arrowhead indicates the boundary between the iodine-positive and -negative areas.

A significant difference was observed in G6P-positive cell rates in each layer between the iodine-positive and -negative areas (*P<0.01, Wilcoxon signed-rank test).

Iodine (+), iodine-positive area; iodine (-), iodine-negative area.

Fig. 5 Immunoreactivity of phosphoglucomutase 3 (PGM3).

(A) and (B): Immunohistochemical expression of PGM3. (C): Comparison of cell positivity rates for PGM in each epithelial layer between the iodine-positive and -negative areas.

(A) Magnification: ×40, (B) Magnification: ×100

The arrowhead indicates the boundary between the iodine-positive and -negative areas.

No significant difference was observed in PGM3-positive cell rates in each layer between the iodine-positive and -negative areas (Wilcoxon signed-rank test).

Iodine (+), iodine-positive area; iodine (-), iodine-negative area

Fig. 6 Metabolome analysis of glycogen metabolism and pentose phosphate pathways.

The concentrations of glutamic acid, arginine, and aspartic acid were significantly higher in OSCC cells than in normal cells. Glycolysis was more strongly activated in normal epithelial cells than in OSCC cells. The concentration of glucose-6-phosphatate was higher in normal epithelial cells than in OSCC cells. The accumulation of lactic acid in OSCC cells may be due to enhanced glutaminolysis, not glycolysis.

Glucose-1-phosphate: G1P, Glucose-6-phosphate: G6P, Fructose-6-phophate: F6P, Fructose-1,6-biphosphate: F1,6P, Glyceraldehyde 3-phosphate: GAP, 1,3-Bisphosphoglycerate: 1,3-DPG, 3-phosphoglyceric acid: 3-PG, 2-phosphoglyceric acid: 2-PG, Phosphoenolpyruvic acid: PEP, 6-phosphogluconic acid: 6PG, Sedoheptulose 7-phosphate: S7P, ribulose-5-phosphate: Ru5P, ribose-5-phosphate: R5P, Phosphoribosyl 1-diphosphate: PRPP.

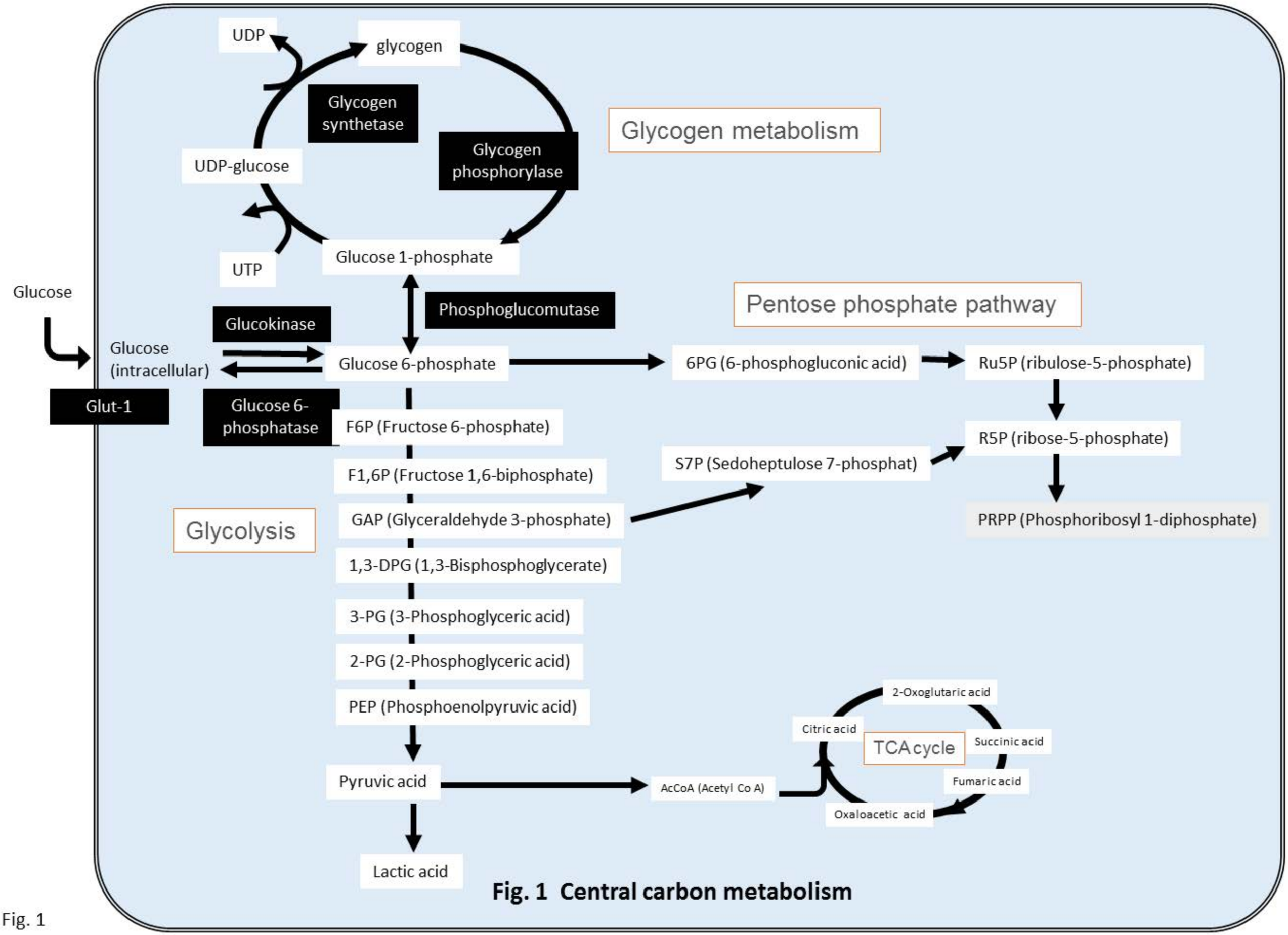

Fig. 1 Central carbon metabolism

Fig. 1

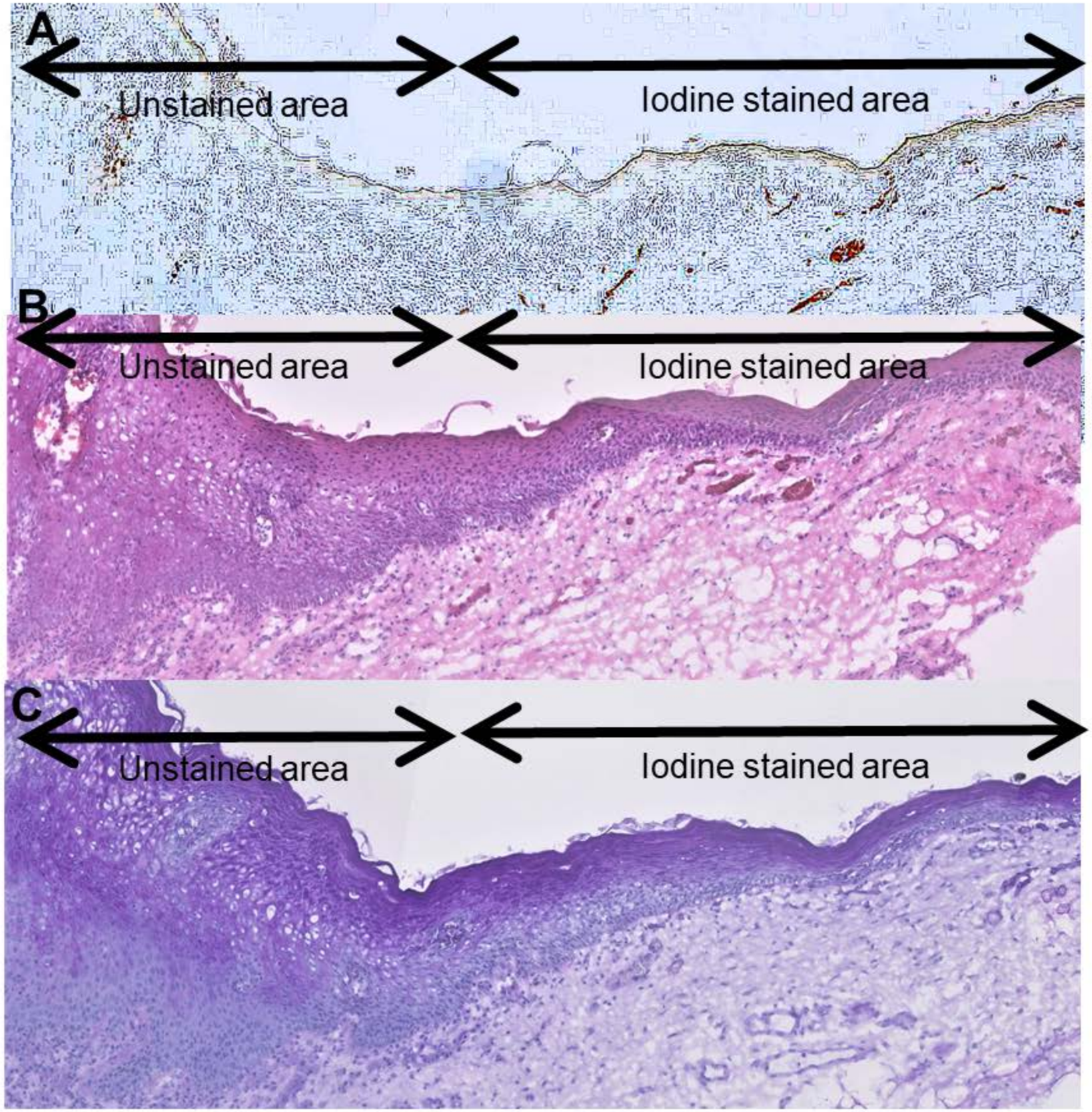

Fig. 2 Iodine stained for frozen tissue section(A), HE staining(B) , and PAS staining(C) (16X)

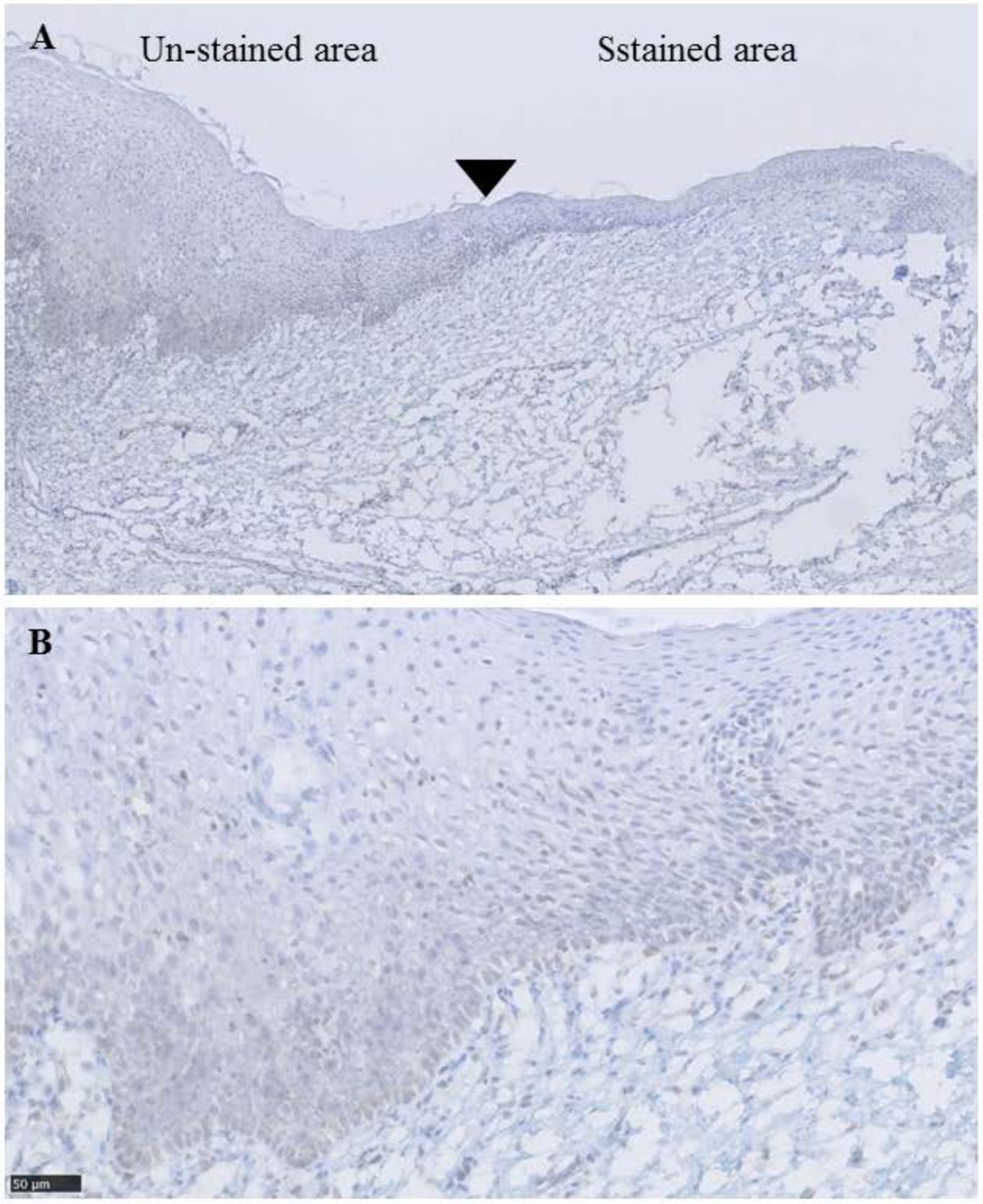

Figure 3. Immunoreaction of glucokinase

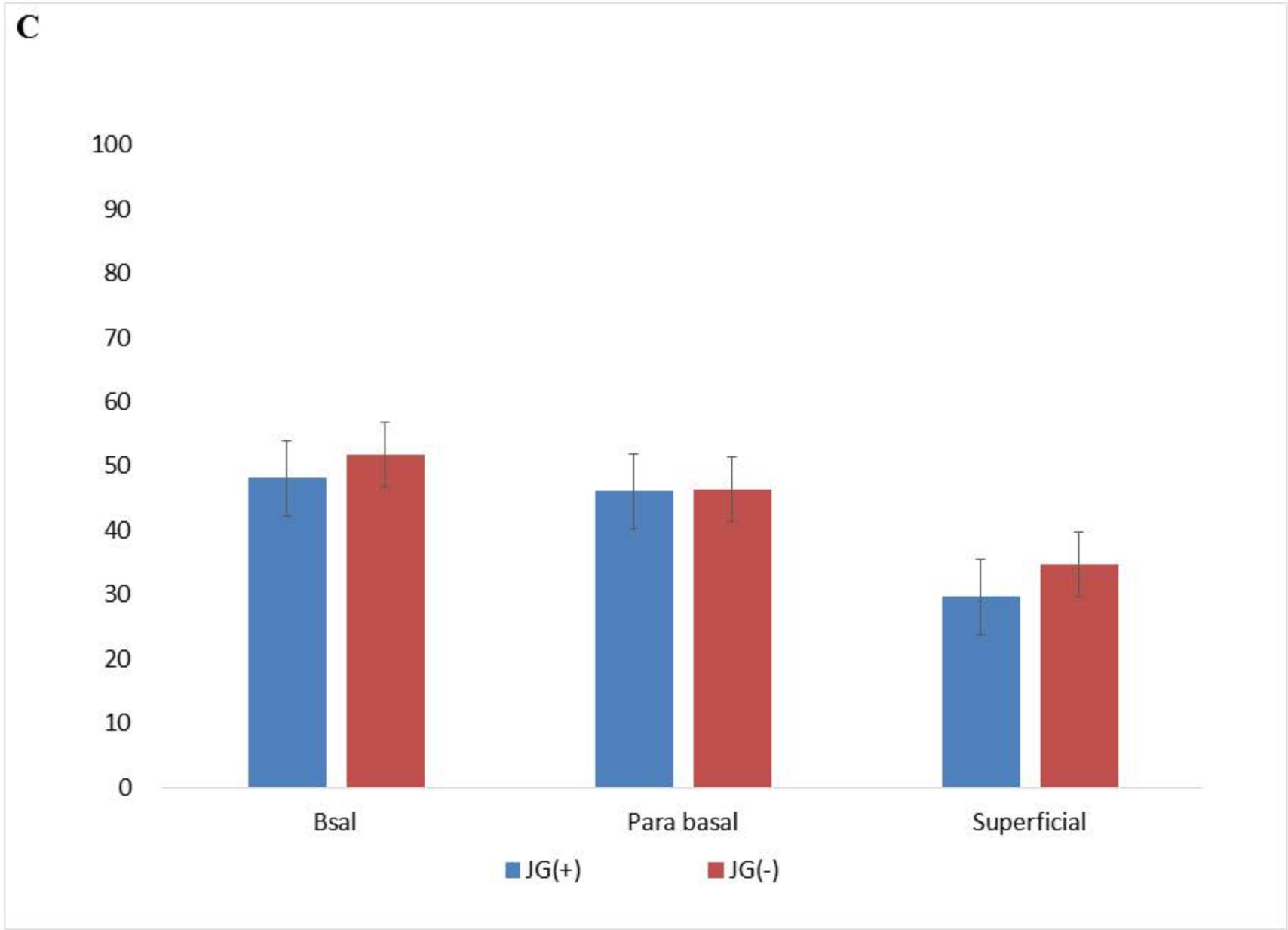

Figure 3. Immunoreaction of glucokinase

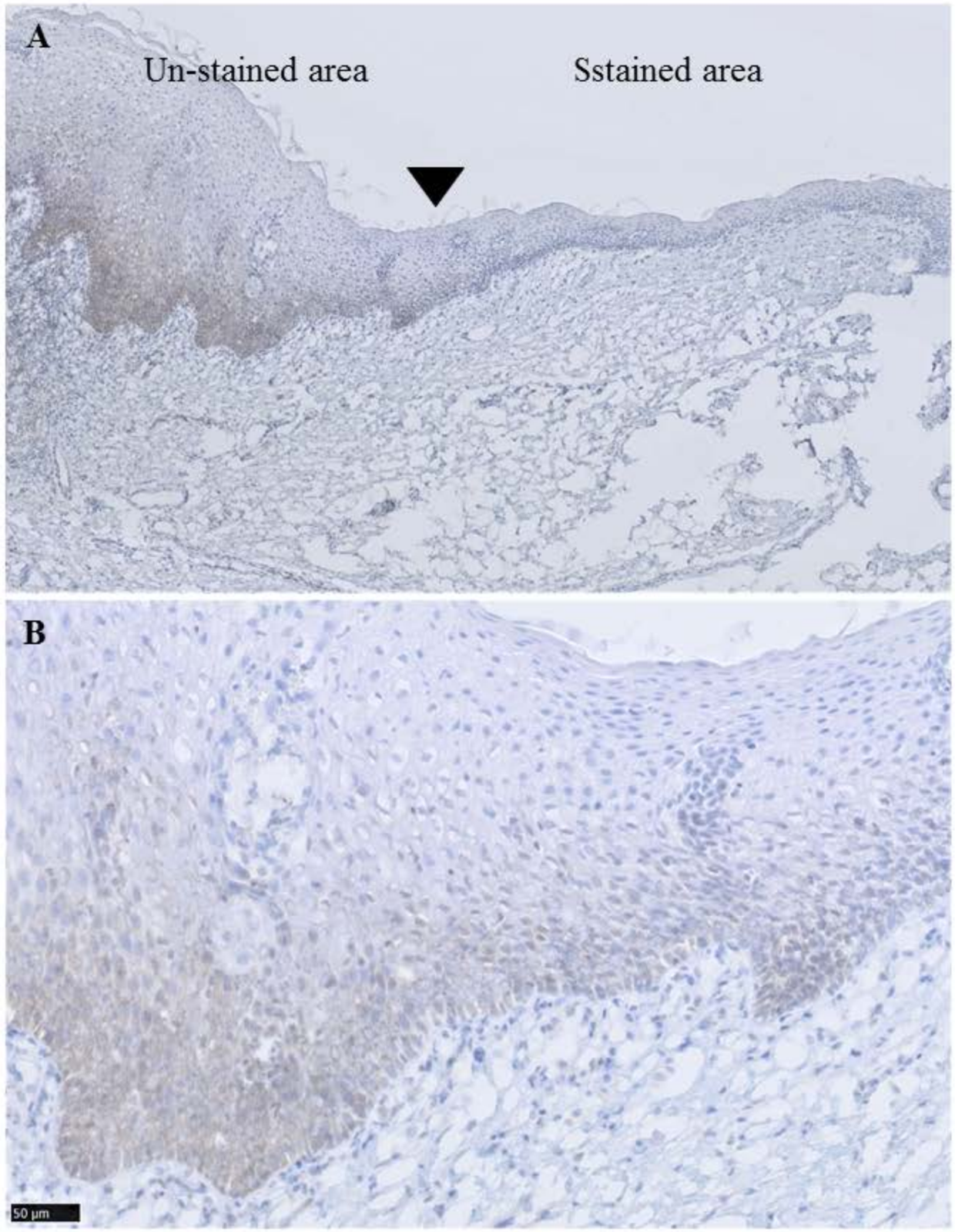

Figure 4. Immunoreactivity of glucose-6-phosphomutase

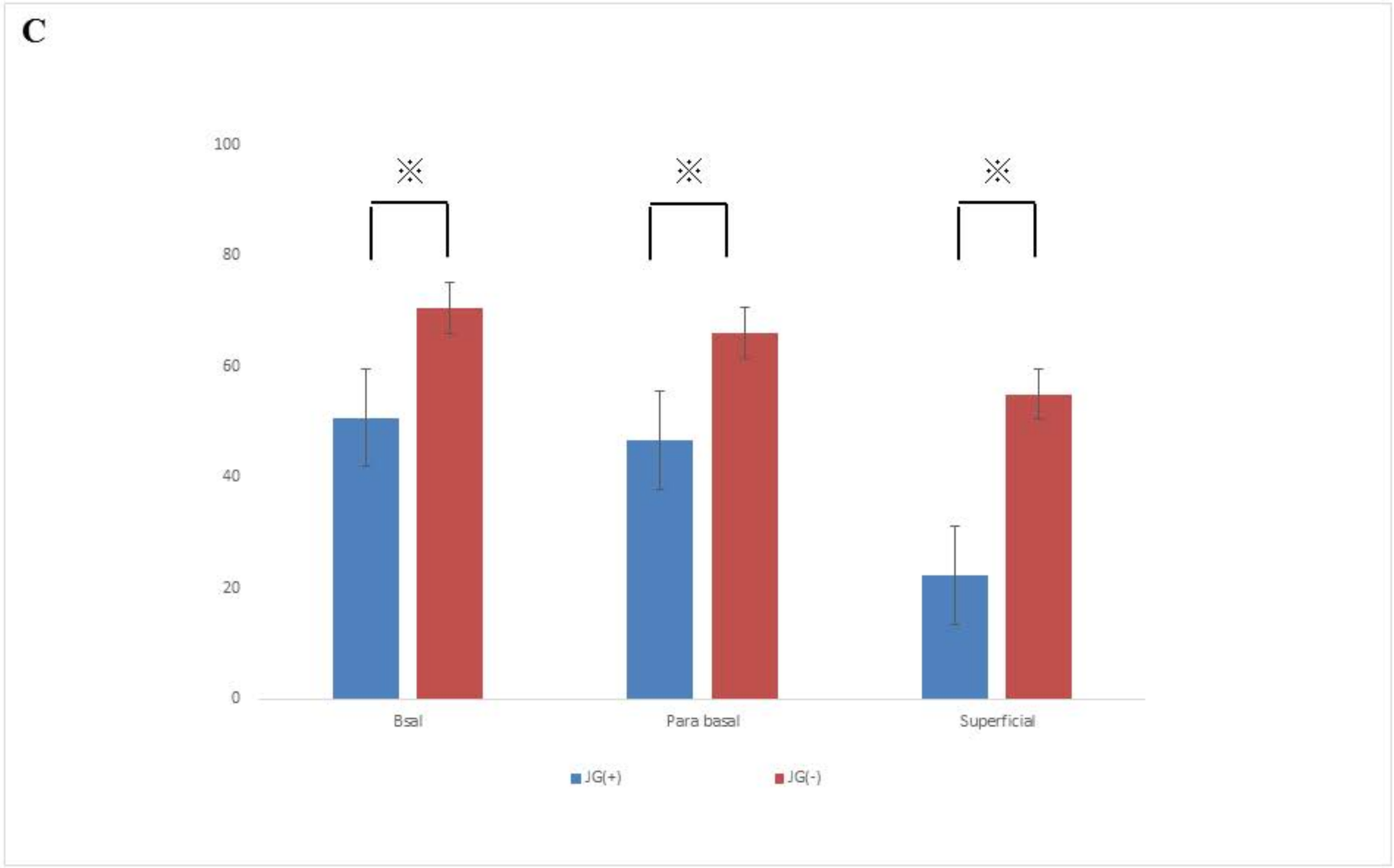

Figure 4. Immunoreactivity of glucose-6-phosphomutase

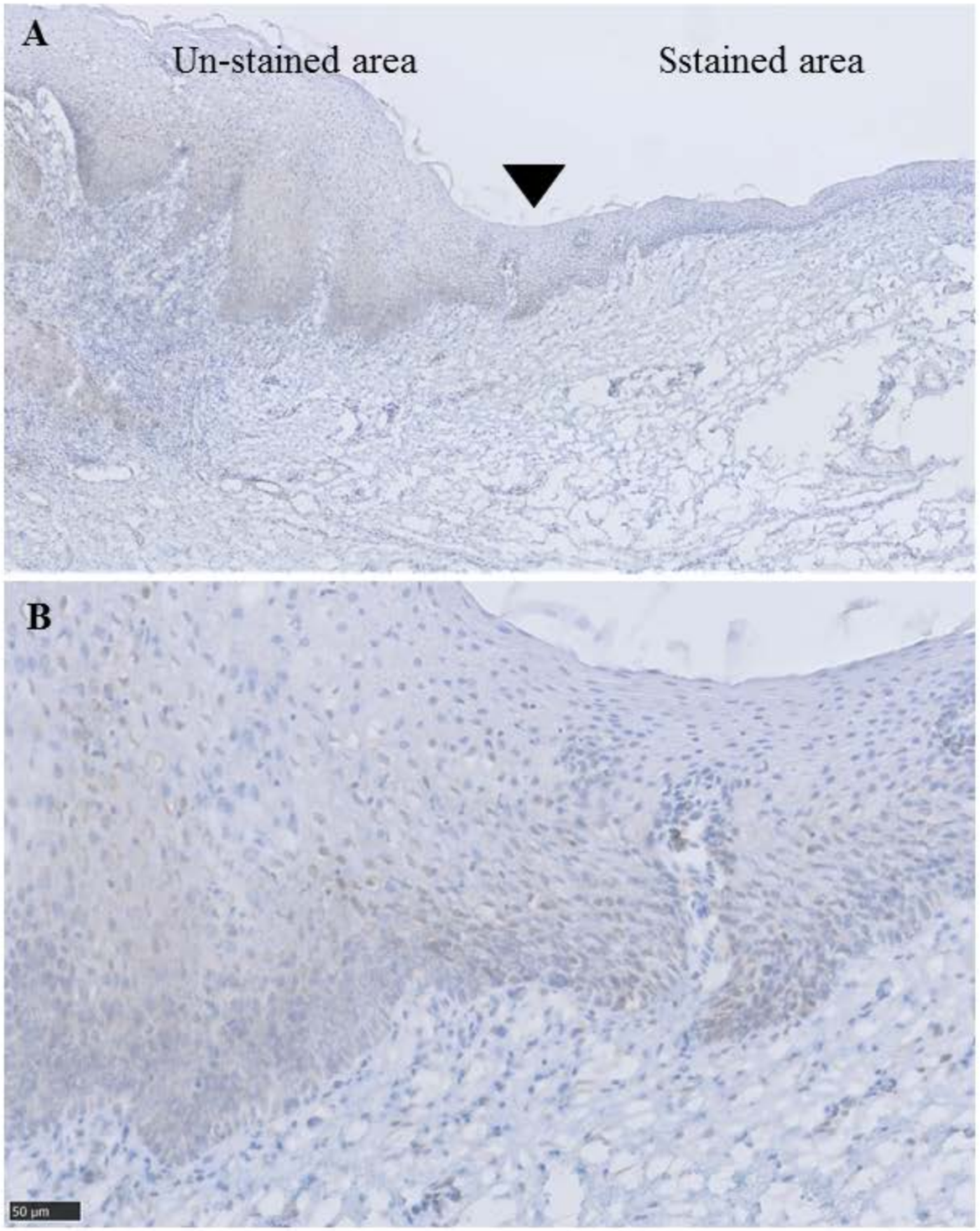

Figure 5. Immunoreactivity of phosphoglucomutase-3

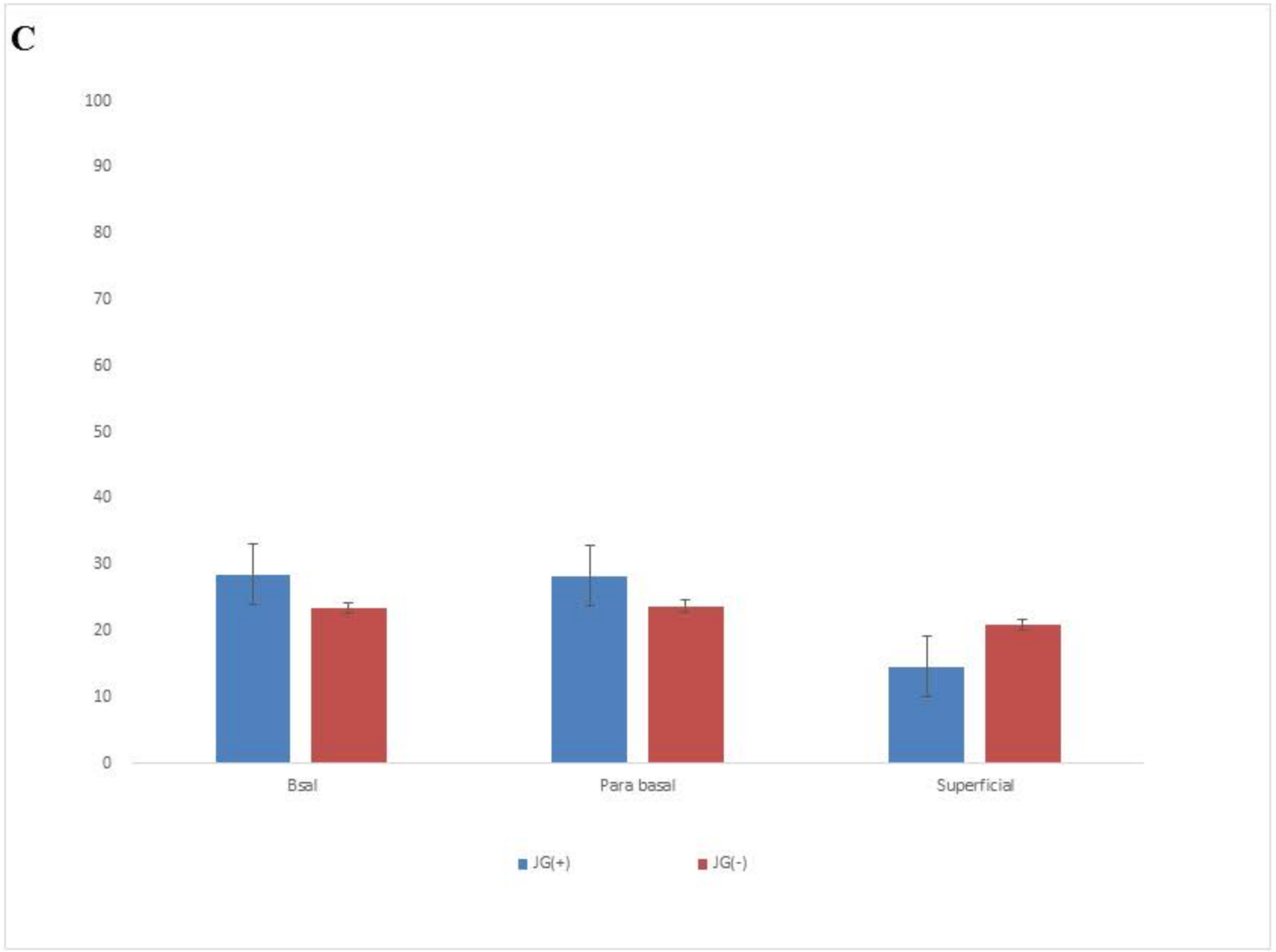

Figure 5. Immunoreactivity of phosphoglucomutase-3

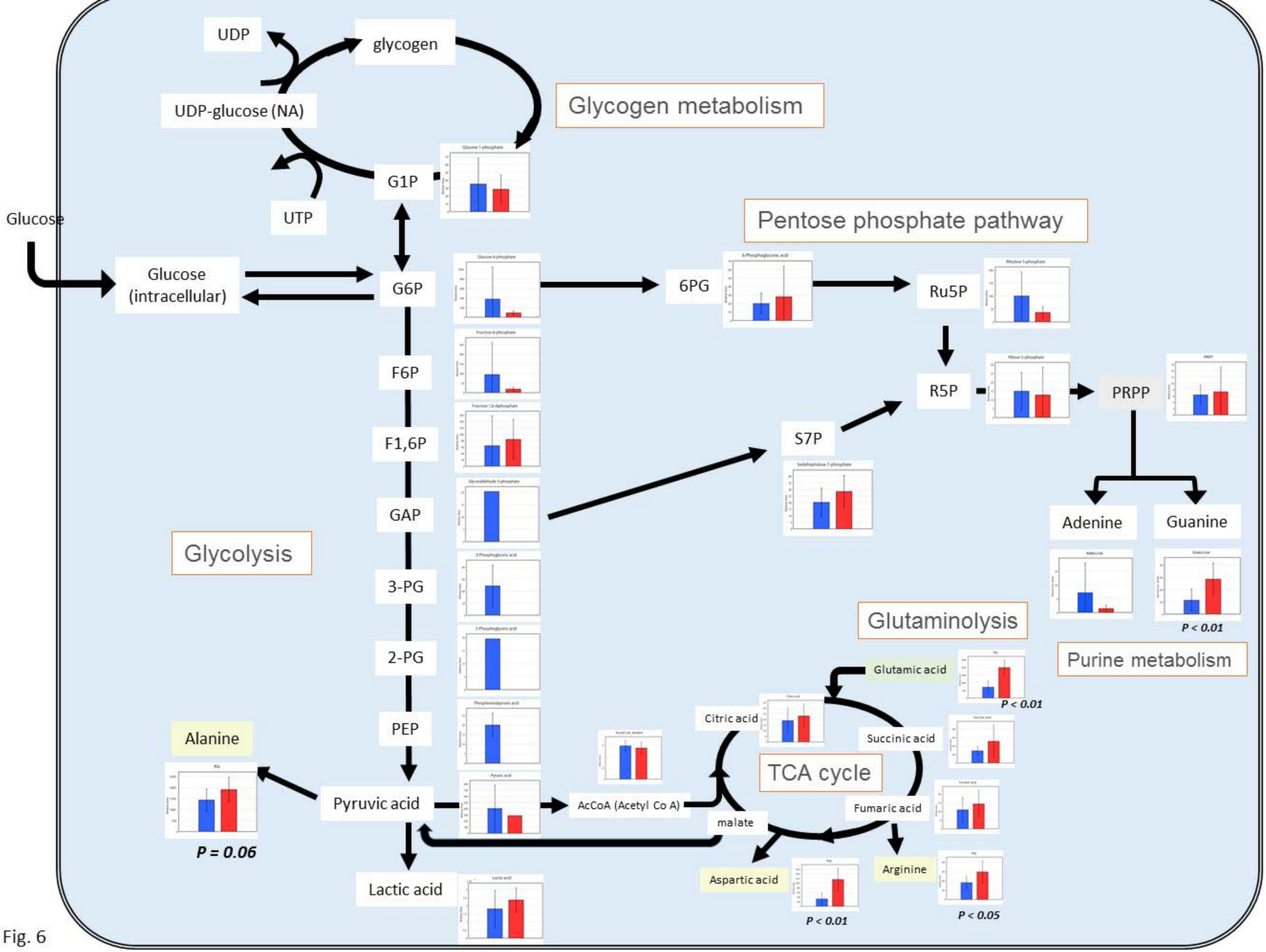
UDP
glycogen
UDP-glucose (NA)
Glycogen metabolism
G1P
UTP
Glucose
Pentose phosphate pathway
Glucose (intracellular)
G6P
6PG
Ru5P
R5P
PRPP
F6P
F1,6P
S7P
GAP
Glycolysis
3-PG
2-PG
PEP
Adenine
Guanine
P < 0.01
Purine metabolism
Glutaminolysis
Glutamic acid
P < 0.01
Citric acid
Succinic acid
TCA cycle
Alanine
Pyruvic acid
AcCoA (Acetyl Co A)
Fumaric acid
malate
Arginine
Aspartic acid
P = 0.06
Lactic acid
P < 0.01
P < 0.05

Fig. 6